Chemical Abundances in Gaseous Nebulae:
Open problems in Nebular astrophysics
AAA Workshop Series 11, 2019
M. Cardaci, G. Hägele & E. Pérez-Montero, eds.

Contributed Paper

The internal kinematic of star-forming regions in interacting galaxies

V. Firpo[1,2], D. Muthukrishna[3], F. Campuzano-Castro[4,5], G. Bosch[4,5], G. Hägele[4,5], S. Torres-Flores[2], & M. Cardaci[4,5]

[1] *Gemini Observatory, Southern Operations Centre,La Serena, Chile.*
[2] *Universidad de La Serena, La Serena, Chile.*
[3] *Institute of Astronomy, University of Cambridge, UK.*
[4] *Instituto de Astrofísica de La Plata, CONICET–UNLP, Argentina.*
[5] *Facultad de Ciencias Astronómicas y Geofísicas, Universidad Nacional de La Plata, Argentina.*

Abstract. Star formation processes can be found in colliding galaxies, where the gas compression can trigger the formation of giant star-forming regions. We present the results from a detailed kinematic analysis in a sample of HII regions located in three strongly interacting galaxies. The velocity dispersion and the luminosity of the multiple-components analyzed in the emission-line profiles suggest that these star-forming objects correspond to giant complexes. In addition, the star formation rates and the ionization state in these regions revealed the presence of ongoing star formation events.

galaxies: kinematics — star formation — ISM

1. Introduction

Interacting galaxies give us a laboratory to study star formation at different levels, ranging from small stellar clusters to Giant HII Regions (GHIIR). The interaction of galaxies increases the turbulence in HIIRs due to the continued accretion of gas onto the HIIRs plus the feedback through stellar winds and supernova explosions (Zaragoza-Cardiel et al., 2015). The knowledge of GHIIR currently remains poor. The early stages of the massive star-forming regions are short-lived, leaving little time for the study of their evolution. Furthermore, there are very few GHIIR per galaxy. Therefore, it is necessary to analyze in detail the few regions available in nearby galaxies and to link the global parameters of these regions with properties such as its gas kinematics, chemical abundances, evolutionary state, and stellar population, which will allow us to expand the study of the GHIIR. In this way, the observations of nearby GHIIRs, with large spectral range and high spectral resolution, provide an excellent laboratory for the study of the important feedback between these regions and their environment.

2. Observation

We have high-resolution spectroscopic from MIKE/echelle, Magellan Telescope (LCO). The spectral ranges (Blue: 3300 Å - 5100 Å, and Red: 4500 Å - 9300 Å) guarantee the measurement of [OII] 3727,29 Å to [SIII] $\lambda\lambda$9069,9532 Å. Resolution obtained at ∼6000 Å is 11∼ km/s (Blue: R∼25000 and Red: R∼20000).

3. Overview and Methodology

We analyze a sample of star-forming regions located in three strongly interacting galaxies NGC 6845, Ap 314, HGC 31.
The analysis of the ionized gaseous component is divided in two parts:

1) kinematical properties (following Firpo et al. (2005, 2010, 2011)): to study line profile asymmetries and multiple components present in the emission lines profiles, determine the radial velocities and the velocity dispersion, estimate luminosities and SFR, and verify the supersonic nature of the ionized gas.
2) physical properties (following Hägele et al. (2006, 2008, 2012)): we estimate electron density and temperature, chemical abundances, reddening, and ionization structure.

The detailed analysis after merging chemical and kinematical information obtained for the gaseous component is called *Chemodynamic* (Esteban & Vilchez, 1992). This analysis is done in the global emission and in the different kinematical components present in all emission-line profiles.

In this work, we present the preliminary results of the first part, where we study the internal kinematic of the ionized gas in six regions by analyzing the multiple kinematical components and the global emission, and confirming (or not) whether these regions have supersonic velocity dispersion.

We developed a complete Python code that automatically models all emission-lines (more-less 30) for all different regions. This code allow us to fit the emission-lines profiles calling the Non-Linear Least-Square Minimization and Curve-Fitting (LMFIT) Python package (Newville et al., 2014). Python's LMFIT iterates over solutions a few hundred times and allow us to obtain better solutions. To determine what is the maximum number of component to fit in the profiles, we use an Akaike Information Criterion indicator (AIC, Akaike, 1974) which allows testing the quality of the statistical model by comparing several models with different Gaussian components, and with different numbers of free parameters.

In summary, this code allows us:

- to find multiple components and/or asymmetric wings in the emission-line profiles,

- to obtain the radial velocities, velocity dispersion, fluxes, emission measure (EM) relative to the total line flux, and the global flux.
- to verify the supersonic nature of the ionized gas for the global and multiple components, and classify the regions as GHIIRs or not.
- to estimate Hα luminosity and Star Formation Rate (Kennicutt, 1998),
- to analyze the ionization source of the objects using the BPT diagnostic diagram (Baldwin et al., 1981),

4. Preliminary Results

High-resolution data are essential to study in detail the internal kinematic and the physical properties of these star forming regions. This data allow us to perform a multiple component analysis on the emission-lines (Firpo et al., 2019 in prep.), which will be enable us to develop a chemodynamical analysis of the strongest star-forming regions located in a sample of interacting systems.
The validity of the profile multiplicity and broadening is checked over the different emission lines. In Figure 4, left panels, we show the plots of the Hα multiple components fit. In the right panels we show the plots of the strongest emission-lines fit. The evident similarity among the different fits in the emission-lines profiles confirms the presence of a complex kinematic structure in all regions.
The width of the emission line profiles give us information regarding supersonic motions. Table 1 shows the average radial velocities and velocity dispersion for the six regions. The velocity dispersion was corrected by instrumental and termal dispersion. Taking account the uncertainties, the global component and the different kinematical components in all regions present supersonic velocity dispersion, typically found in GHIIRs. The exception is the Narrow 1 component in HCG 31-C region, that we have estimated a velocity dispersion of 7.1 ± 4.2 km s^{-1}.

Table 1. Average radial velocities and velocity dispersion for different components in all regions.

	v_r (km s^{-1})	σ (km s^{-1})	v_r (km s^{-1})	σ (km s^{-1})
	HCG31-A		HCG31-C	
Narrow 1	4023.0 ± 1.5	16.3 ± 2.7	3918.3 ± 3.3	7.1 ± 4.2
Narrow 2	4001.7 ± 3.1	40.5 ± 2.3	3975.2 ± 2.0	40.4 ± 2.2
Broad	3977.9 ± 4.6	94.2 ± 4.1	4006.9 ± 2.3	87.6 ± 6.6
	NGC6845-7		NGC6845-26	
Narrow 1	6312.4 ± 2.4	16.7 ± 1.5	6169.2 ± 1.2	14.7 ± 2.5
Narrow 2	6348.1 ± 2.8	11.8 ± 1.5	6192.4 ± 3.2	49.7 ± 2.7
Broad	6327.6 ± 1.8	55.2 ± 1.9	6195.8 ± 5.3	125.4 ± 10.6
	Arp314-NED02		Arp314-NED02-off	
Narrow 1	3651.3 ± 1.5	35.7 ± 3.5	3655.8 ± 1.9	37.0 ± 2.7
Narrow 2	3663.5 ± 2.0	13.1 ± 2.3	3663.9 ± 2.2	15.9 ± 2.5
Broad	3644.9 ± 8.9	71.3 ± 7.8	3651.9 ± 7.6	71.0 ± 3.4

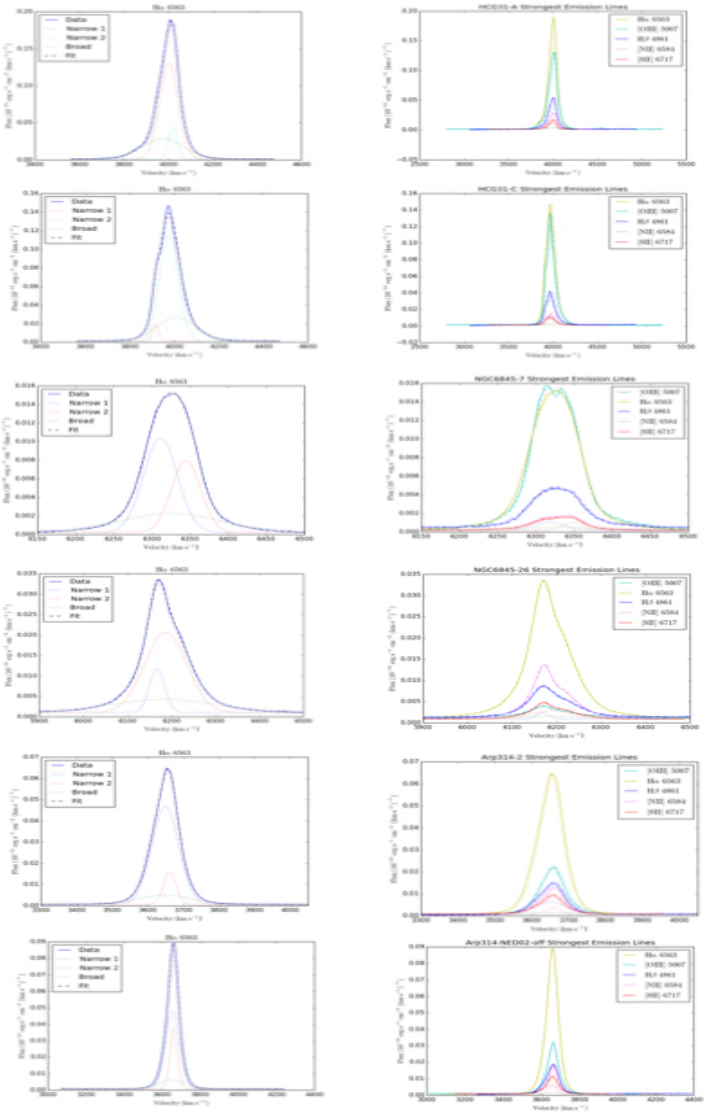

Figure 1. Left panels: Hα multiple components fit. Right panels: The strongest emission-lines fit.

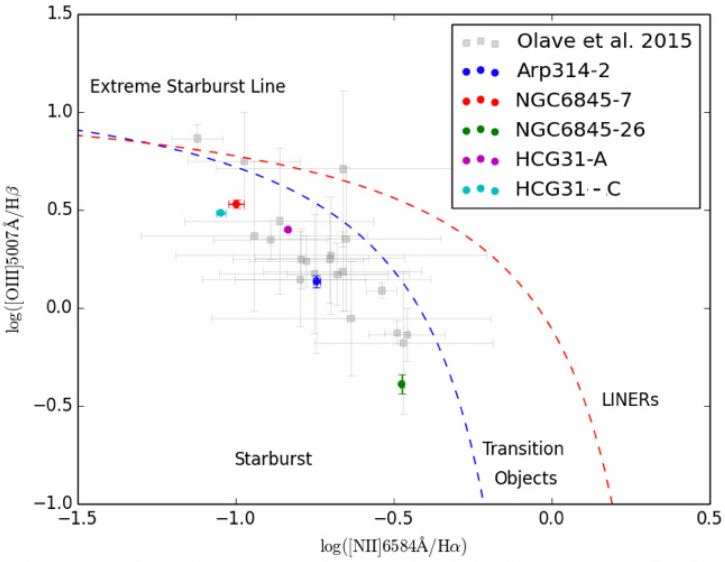

Figure 2. BPT diagnostic diagram for the global Gaussian component of each star-forming region. The regions studied in Olave-Rojas et al. (2015) are overlapped in grey squares.

In Figure 4, we show the BPT diagnostic diagram for the global Gaussian component of each star-forming region. This diagnostic diagram shows that all studied regions are ionized by massive stars.
In table 2, we show the SFR and Hα luminosities for all regions. This values are typical of giant star-forming complexes.

Table 2. SFR and logaritm of Hα luminosities for the six regions.

Region Name	SFR ($M_\odot$ yr^{-1})	log(L(Hα)) ($ergs^{-1}$)
HCG31-A	0.42 ± 0.003	40.9 ± 0.003
HCG31-C	0.35 ± 0.004	40.8 ± 0.005
NGC6845-7	0.04 ± 0.001	39.9 ± 0.006
NGC6845-26	0.08 ± 0.000	40.2 ± 0.002
Arp314-NED02	0.11 ± 0.001	40.3 ± 0.003
Arp314-NED02-off	0.13 ± 0.001	40.4 ± 0.005

Acknowledgments. VF acknowledges support from CONICYT Astronomy Program-2015 Research Fellow GEMINI-CONICYT (32RF0002).

References

Akaike H., 1974, *IEEE Transactions on Automatic Control*, **19**, 716
Baldwin J. A., Phillips M. M., Terlevich R., 1981, *PASP*, **93**, 5
Esteban C., Vilchez J. M., 1992, *ApJ*, **390**, 536
Firpo V., Bosch G., Hägele G. F., Díaz Á. I., Morrell N., 2011, *MNRAS*, **414**, 3288
Firpo V., Bosch G., Hägele G. F., Morrell N., 2010, *MNRAS*, **406**, 1094
Firpo V., Bosch G., Morrell N., 2005, *MNRAS*, **356**, 1357
Hägele G. F., Díaz Á. I., Terlevich E., Terlevich R., Pérez-Montero E., Cardaci M. V., 2008, *MNRAS*, **383**, 209
Hägele G. F., Firpo V., Bosch G., Díaz Á. I., Morrell N., 2012, *MNRAS*, **422**, 3475
Hägele G. F., Pérez-Montero E., Díaz Á. I., Terlevich E., Terlevich R., 2006, *MNRAS*, **372**, 293
Kennicutt Jr. R. C., 1998, *ARA&A*, **36**, 189
Newville M., Stensitzki T., Allen D. B., Ingargiola A., 2014, *LMFIT: Non-Linear Least-Square Minimization and Curve-Fitting for Python*
Olave-Rojas D., Torres-Flores S., Carrasco E. R., Mendes de Oliveira C., de Mello D. F., Scarano S., 2015, *MNRAS*, **453**, 2808
Zaragoza-Cardiel J., Beckman J. E., Font J., García-Lorenzo B., Camps-Fariña A., Fathi K., James P. A., Erroz-Ferrer S., Barrera-Ballesteros J., Cisternas M., 2015, *MNRAS*, **451**, 1307